The Astrophysical Journal, 610:1148–1156, 2004 August 1

ILCT: RECOVERING PHOTOSPHERIC VELOCITIES FROM MAGNETOGRAMS BY COMBINING THE INDUCTION EQUATION WITH LOCAL CORRELATION TRACKING

B. T. Welsch, G. H. Fisher, and W. P. Abbett
Space Sciences Laboratory, University of California, Berkeley, CA 94720-7450; welsch@ssl.berkeley.edu

and

S. Regnier
Department of Physics, Montana State University, Bozeman, MT 59717-3840
Received 2004 February 2; accepted 2004 April 9

ABSTRACT

We present three methods for deriving the velocity field in magnetized regions of the Sun's photosphere. As a preliminary step, we introduce a Fourier-based local correlation tracking (LCT) routine that we term "FLCT." By explicitly employing the observation made by Démoulin & Berger, that results determined by LCT applied to magnetograms involve a combination of all components of the velocity and magnetic fields, we show that a three-component velocity field can be derived, in a method we term algebraic decomposition, or ADC. Finally, we introduce ILCT, a method that enforces consistency between the normal component of the induction equation and results obtained from LCT. When used with photospheric vector magnetograms, ILCT determines a three-component photospheric velocity field suitable for use with time sequences of such magnetograms to drive boundary conditions for MHD simulations of the solar corona. We present results from these methods applied to vector magnetograms of NOAA AR 8210 on 1998 May 1.

Subject headings: methods: data analysis — Sun: atmospheric motions — Sun: magnetic fields — Sun: photosphere

On-line material: mpeg animations

1. WHY INVESTIGATE PHOTOSPHERIC VELOCITIES?

How are solar observational data used in theoretical or numerical modeling of eruptive events in solar physics? Observations from instruments such as the *SOHO* Michelson Doppler Imager (MDI) and Extreme-Ultraviolet Imaging Telescope (EIT), *TRACE*, or the *GOES* Solar X-Ray Imager (SXI) provide qualitative descriptions of the morphological evolution of the Sun's magnetic field and atmospheric structure. A more quantitative approach is to apply force-free (Démoulin et al. 1997) or potential (Luhmann et al. 1998) field extrapolations to a time series of photospheric magnetograms, and to study the evolution of the extrapolations' topological structure with time.

Such methods, however, cannot show how the coronal field evolves continuously in response to changes in the vector magnetic field at the photosphere (Li et al. 2001). In contrast, MHD models *are* capable of modeling the coronal field's topological evolution, but require specification of an electric field consistent with the observed evolution of the magnetic field at the photospheric boundary. While some studies of the large-scale outer corona (Roussev et al. 2003; Riley et al. 2001) incorporate line-of-sight magnetograms into the bottom boundary of time-dependent MHD solar wind solutions, no method of incorporating time-varying *vector* magnetogram data into MHD models of the corona has been developed. In this paper, we present a first step in this direction: a technique to determine a velocity field at the photosphere that is physically consistent with a given time series of vector magnetogram observations. This velocity field can be used to derive an electric field consistent with observations and suitable for driving coronal MHD simulations.

In § 2, we describe a 4 hr series of vector magnetograms of NOAA AR 8210, to which we will apply our technique. A flare and coronal mass ejection (CME) began at 22:30 UT on 1998 May 1, soon after this magnetogram sequence ended at 21:29. This active region is of special interest because it produced a large number of flares and eruptive events during its transit across the solar disk, and has been the subject of many other studies (Sterling & Moore 2001; Sterling et al. 2001; Pohjolainen et al. 2001; Wang et al. 2002; Warmuth et al. 2000; Xia et al. 2002). In the same section, we also present a "data movie" we made of AR 8210's line-of-sight field on 1 May 1998, from MDI full-disk data. We start § 3 with a discussion of local correlation tracking (LCT), and in particular its application to magnetograms. We then present a Fourier-based LCT routine (FLCT) and show FLCT results from the vector magnetogram data, as well as results from the MDI data, in the form of an "LCT movie." This is followed by a discussion of the magnetic induction equation, and the constraints it places on the flow field. We then discuss how flows both perpendicular and parallel to the magnetogram surface can be derived by simple algebra if vector magnetogram data are available, a technique we term algebraic decomposition, or ADC. Finally, we present the induction LCT (ILCT) method of deriving three-component photospheric velocities, which enforces consistency between the ideal induction's normal component and results from LCT. We conclude in § 4 by applying the ILCT technique to the AR 8210 data, and discuss our results and their implications.

2. THE DATA

To determine photospheric motions we use a time series of vector magnetograms taken by the Imaging Vector Magnetograph (IVM; Mickey et al. 1996; Kupke et al. 2000) at the Mees Solar Observatory. The instrument measures the four Stokes parameters

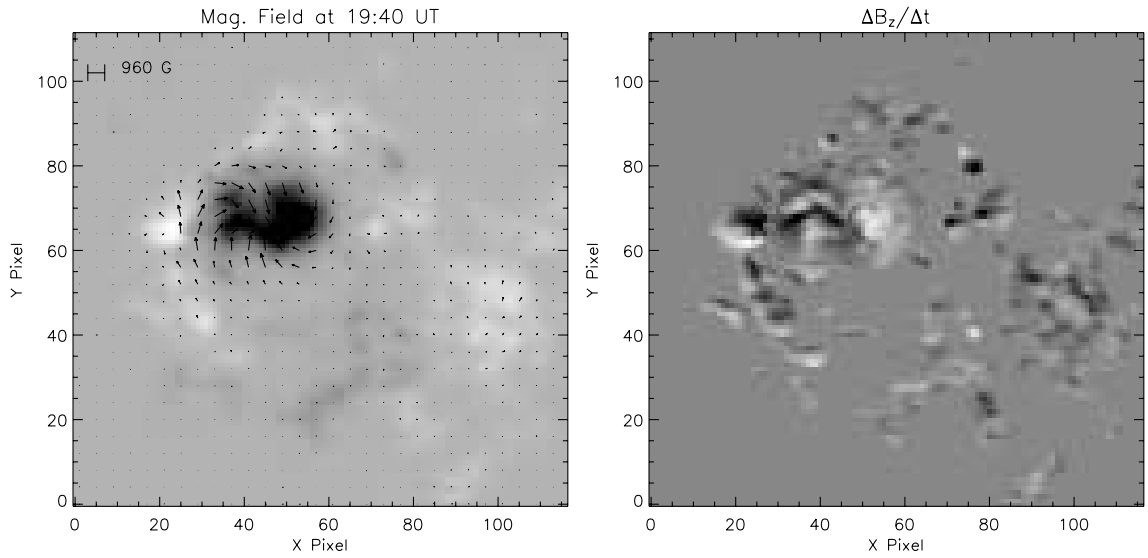

FIG. 1.—*Left*: Magnetic field in NOAA AR 8210 at 19:40 UT on 1998 May 1, with B_z in gray scale and $\boldsymbol{B}_t$ in vectors (the density of vectors has been reduced for visualization). *Right*: Difference, ΔB_z, in the normal component of the field between 21:29 UT and 17:13 UT on 1998 May 1.

of the photospheric Fe I line at 6302.5 Å, which are used to deduce the three components of the magnetic field. This inversion is based on the Unno (1956) fitting method by applying Auer (1977) equations to derive the magnetic field and including magneto-optic effects after Landolfi & Landi Degl'Innocenti (1982). The derived vector magnetic field is then transformed in the disk-center heliographic frame after the resolution of the 180° ambiguity existing in the transverse component (Canfield et al. 1993).

The data set was obtained on 1998 May 1 for AR 8210 (S16 E02 at 17:00 UT). To reduce the noise level, we have averaged five consecutive records of Stokes parameters to produce averaged vector magnetograms. We thus obtain a time series of 15 vector magnetograms with an average cadence of 18 minutes, from 17:13 UT to 21:29 UT. The pixels were originally 1.″1 square, but, for the sake of comparison with other models (Régnier et al. 2002), we put the magnetic data on a 117×112 pixel grid, with an effective pixel size of 1.″77 (~1280 km). For all magnetograms in the sequence, the normal component of the field in the $(i + 1)$th magnetogram was cross-correlated with that in the ith magnetogram, and all field components were shifted accordingly for precise co-alignment. As an example, we show the photospheric vector magnetic field for AR 8210 at 19:40 UT on 1998 May 1 in the left panel of Figure 1.

The dynamic evolution of the active region was studied using a "data movie" created from a subregion of MDI/SOI (Scherrer et al. 1995) full-disk magnetograms, and is available as an mpeg animation in the electronic version of this paper.[1] It was made from a series of 96 temporal averages over 15 images taken with a nominal 1 minute cadence, starting at 10:30:04 UT on 1998 May 1, and continuing for slightly more than 24 hr (when data gaps occurred, subsequent images were used). Crude derotation was effected by advancing the boundaries of the subregion in time. The movie highlights several interesting features:

1. The main sunspot (negative polarity) is rotating clockwise.
2. On the northwest part of AR 8210, a newly emerged negative polarity is moving quickly toward the southwest.
3. The northern end of AR 8210 exhibits convergence and cancellation of oppositely signed flux.

3. THE METHOD

3.1. *FLCT: Local Correlation Tracking*

The various LCT schema in widespread use today have one central idea: proper motions of intensity features in successive images—whether G-band filtergrams, Hα images, or photospheric magnetograms—separated in time by Δt are found by maximizing a cross-correlation function, or minimizing an error function between subregions of the images.

The concept of LCT is generally attributed to November & Simon (1988). Their method shifts images at nine integer-pixel spatial lags (one null, and eight toward nearest-neighbor pixels) and computes a cross-correlation at each shift. Their cross-correlation is the integrated product of a Gaussian windowing function with the smoothed before and after images at a given shift. To get subpixel resolution, they use biquadratic interpolation on the nine-point cross-correlation distribution to determine which shift coincides with the maximum correlation. Multiplying by pixel size and dividing by Δt results in a velocity.

Another well-known method minimizes the rms error between corresponding subimages, or "tiles" as they are frequently called, as described by Berger et al. (1998). Each subimage from one image is shifted until it is most closely aligned with the corresponding subimage from the other image. When the shifts have been optimized, the pattern of subimage shifts reveals the motion that occurred over Δt, and the overall velocity pattern can be determined by interpolating between the shifts of the tiles.

[1] The movie can also be retrieved at http://solarmuri.ssl.berkeley.edu/~welsch/public/data/8210/8210_MDI.mpg, or by request.

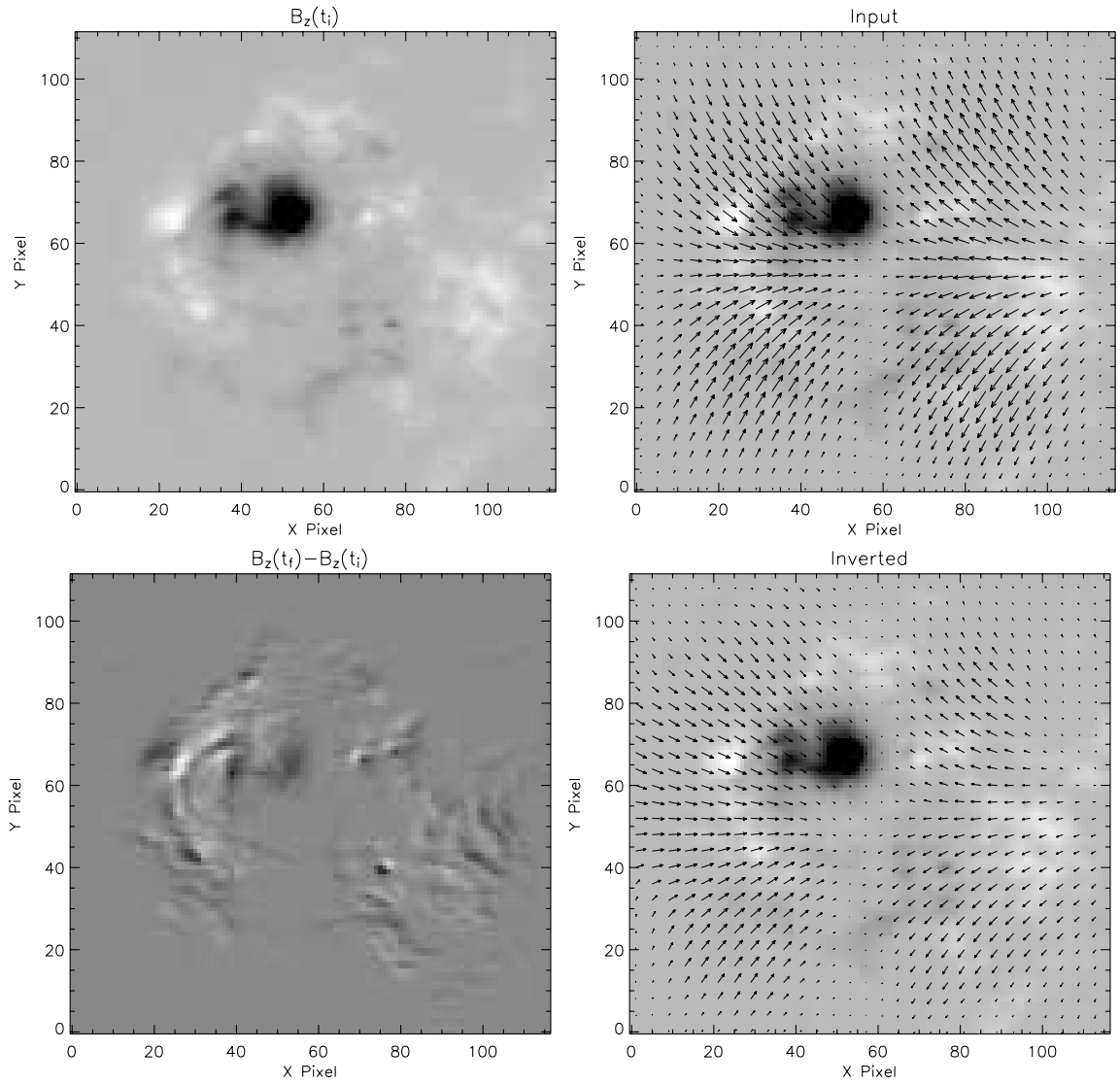

FIG. 2.—Here we show results from a numerical experiment to test our LCT method. The image at top left is the normal field, B_z, at 19:40 UT. Using the input velocity field shown at top right with a two-dimensional advection code, we evolved B_z such that the difference between advected and original fields, ΔB_z, shown at bottom left, resulted. The inverted velocity field, determined by LCT, is shown at bottom right. Input and inverted velocity vectors are shown with the same normalization. (Both vector fields are shown at reduced resolution for visualization.)

LCT results presented here were obtained using a method we developed ourselves, FLCT, which employs Fourier correlation.[2] For each pixel in the image array, we:

1. multiply each of the images to be correlated (call them images 1 and 2) by a Gaussian, of width σ, centered at that pixel;
2. crop the resulting altered images 1 and 2 by chopping off the insignificant parts of the images, reducing image size and thereby dramatically increasing computational speed;
3. compute the cross-correlation function between the two cropped images using standard fast Fourier transform (FFT) techniques;
4. use cubic-convolution interpolation to find the shifts in x and y that maximize the cross-correlation function to one of two precisions (chosen by the user), either 0.1 or 0.02 pixel; and
5. use the shifts in x and y and Δt between images to find the intensity features' velocities along the solar surface.

While the procedure sounds different from that described in November & Simon (1988) and Berger et al. (1998), tests we have done thus far reveal that all of the methods behave similarly. The quantity σ in our method is analogous to the "tile size" in Berger et al. (1998).

We ultimately want to determine the flow that affects the photospheric footpoints of coronal fields. Thus, the appropriate correlation for our purposes is between the normal field intensities obtained from vector magnetograms. We demonstrate our LCT method in a numerical experiment, using an IVM magnetogram from the sequence described in § 2. For this "moving

[2] Our procedure was written in IDL, and the two relevant codes, vel_ccor.pro and cross_cor.pro, can be found at http://solarmuri.ssl.berkeley.edu/overview/publicdownloads/software.html.

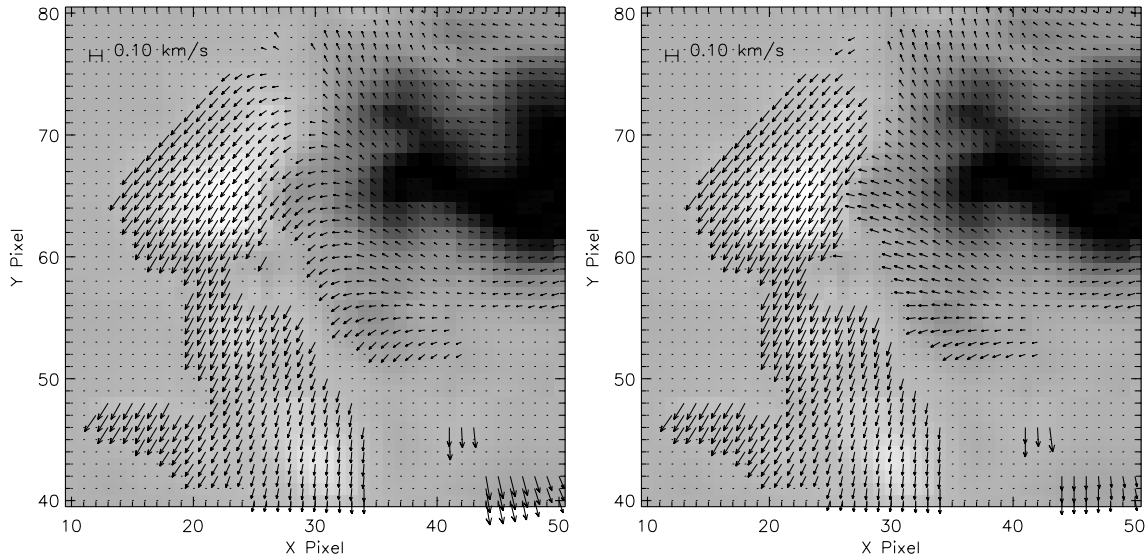

FIG. 3.—Comparison of velocities in a subregion of AR 8210 data near a neutral line. Velocities at left were found via LCT on both polarities simultaneously, while those at right were found by combining results from separate LCT runs on each polarity. The subregion encompasses pixels with $x \in (10:50)$ and $y \in (40:80)$ in Fig. 1.

paint'' experiment, we take an initial $(N_x \times N_y)$ array of B_z values at time t_i, and use a simple two-dimensional predictor-corrector code to advect them with assumed velocities at pixel (j, k) given by $v_x(j, k) = \sin(\pi j/N_x) \sin(2\pi k/N_y)$ and $v_y(j, k) = \sin(2\pi j/N_x) \sin(2\pi k/N_y)$. This yields a second B_z array at a ''time'' t_f. Using FLCT code on the two images, with $\sigma = 15$ pixels, we can approximately reconstruct the imposed flows, as shown in Figure 2. We observe that, in all such two-dimensional, kinematic experiments we have performed, our simple advection code appears to diminish the imposed flows by about $\sim$10% (when compared to integer array shifts), and FLCT underestimates the imposed flows by $\lesssim$10%. This compares well with published error estimates for other LCT codes (Simon et al. 1995; Strous 1995).

This test and others performed thus far suggest that FLCT results reasonably approximate an applied velocity field if:

1. the spatial scale of structures in the image is small compared to the spatial scale over which the velocity varies, and
2. σ is large compared to the spatial scale of features in the image.

In practice, the rich structure in solar magnetograms generally allows imposed flows to be recovered accurately.

We find, in general, that noisy fluctuations in regions of weak normal field lead to spurious correlations there. For this reason, we disregard correlations in such regions: in the AR 8210 magnetograms, we discard velocities in regions where $|B_z| < 100$ G. In general, we also ignore velocities greater than 5 km s^{-1} (near the photospheric sound speed), although none of the LCT runs in this work returned such large velocities. We also found that Δt between correlated magnetograms had to be large enough that mean changes in B_z exceeded fluctuations in B_z. Assuming velocities $\sim$1 km s^{-1}, with 1280 km wide pixels in our IVM data, steady flows should change field structures on scales of 3 pixels over the course of an hour. To ensure the strongest possible signal, we correlated the first and last magnetograms in the sequence, meaning Δt was 4 hr, 16 minutes. We set $\sigma = 10$ pixels.

The data movie discussed in § 2 also clearly shows opposite-polarity fields at the active region's eastern edge moving independently of each other, even in close proximity. We suspected that this led to crosstalk in the correlations, affecting LCT velocities near neutral lines. Accordingly, we applied FLCT separately to each polarity in this work, and combined the results from each mask. Results obtained by tracking polarities simultaneously and separately are shown in Figure 3.

We also applied the FLCT method to the line-of-sight field data from MDI used to make the movie discussed in § 2, and have generated an ''LCT movie'' (available as an mpeg animation in the electronic version of this paper).[3] Here, we have applied our technique to magnetograms 15 steps (or $\sim$255 minutes) apart, and have overlaid the resulting velocity field onto the sequence of images. In the concluding section of this paper, we compare this FLCT flow field with the flow field obtained using ILCT, the technique we introduce in § 3.4.

3.2. *The Démoulin & Berger Relation*

Démoulin & Berger (2003) observed that the apparent horizontal velocity field of intensity features in magnetograms, $\boldsymbol{u}$, is not necessarily identical to plasma velocity field tangent to the surface, $\boldsymbol{v}_t$, although others have treated the two as equivalent. Instead, from a geometrical argument, they derive

$$\boldsymbol{u} = \boldsymbol{v}_t - \boldsymbol{B}_t v_n / B_n. \tag{1}$$

Here, the components of vectors normal to or tangent to the photosphere are denoted by the subscripts n and t, respectively. They note that the flow field from LCT, $\boldsymbol{u}^{(\mathrm{LCT})}$, is an estimate of $\boldsymbol{u}$, and briefly discuss the inaccuracies of using LCT with magnetograms.

[3] The movie can also be retrieved at http://solarmuri.ssl.berkeley.edu/~welsch/public/data/8210/8210_LCT.mpg, or by request.

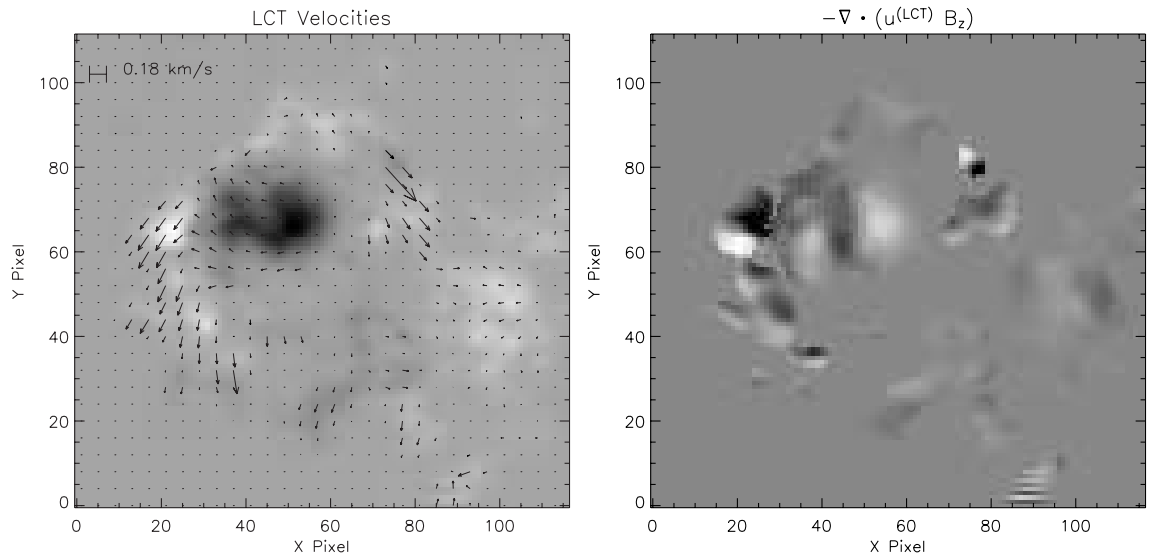

FIG. 4.—*Left*: LCT velocities determined from magnetograms at 17:13 and 21:29 UT on 1998 May 1. *Right*: $-\nabla_t \cdot [\boldsymbol{u}^{(\mathrm{LCT})}\bar{B}_z]$. Démoulin & Berger (2003) suggest that the right panel of this figure should closely approximate the change in normal field, ΔB_z, shown in the right panel of Fig. 1. While the panels show similarities, the differences are significant enough to affect an MHD simulation.

When applied to magnetograms, LCT is intimately related to the time evolution of the field's normal component, which is governed by the induction equation. As an approximation, we assume field evolution consistent with ideal MHD at the photosphere, or

$$\frac{\partial \boldsymbol{B}}{\partial t} = \nabla \times (\boldsymbol{v} \times \boldsymbol{B}). \tag{2}$$

We assume that vector magnetograms specify the field components at a given height in the atmosphere. Since the transverse components of the induction equation contain derivatives in the normal direction (which we cannot determine observationally without measurements at two different heights in the atmosphere), we consider only the normal component of equation (2):

$$\frac{\partial B_n}{\partial t} = \nabla_t \cdot (v_n \boldsymbol{B}_t - B_n \boldsymbol{v}_t). \tag{3}$$

Note that $\partial B_n/\partial t$ can be regarded as a combination of a flux emergence term and a horizontal transport term.

Equation (1) implies that $\boldsymbol{u}\bar{B}_n$ can be substituted into a temporal finite-difference approximation to equation (3),

$$\frac{\Delta B_n}{\Delta t} = \nabla_t \cdot (v_n \bar{\boldsymbol{B}}_t - \bar{B}_n \boldsymbol{v}_t), \tag{4}$$

to give

$$\Delta B_n/\Delta t = -\nabla_t \cdot (\boldsymbol{u}\bar{B}_n) \simeq -\nabla_t \cdot \left[\boldsymbol{u}^{(\mathrm{LCT})}\bar{B}_n\right]. \tag{5}$$

The overbar on the magnetic field components in these expressions refers either to a temporal average of fields between the times t_i and t_{i+1} used in LCT, or to the measured field at an intermediate time, $t_{i+1/2}$. In this work, we adopt the latter approach.

In addition to the errors introduced by making the ideal and finite-difference approximations, $\Delta B_n/\Delta t$ and $-\nabla_t \cdot [\boldsymbol{u}^{(\mathrm{LCT})}\bar{B}_n]$ can disagree because they are determined independently from each pair of magnetograms. These differences are illustrated for the case of AR 8210 in Figure 4.

3.3. *ADC: Finding* $\boldsymbol{v}$ *from* $\boldsymbol{u}^{(\mathrm{LCT})}$ *and* $\boldsymbol{B}$

Equation (1) provides two relations among the three unknown components of $\boldsymbol{v}$ at the photosphere, if we assume that $\boldsymbol{B}$ is known and that $\boldsymbol{u} \simeq \boldsymbol{u}^{(\mathrm{LCT})}$. Determination of the three components of the photospheric velocity vector therefore requires either additional data or additional assumptions regarding the available data. For instance, Doppler measurements, when these data happen to exist, can determine v_n. In cases where such data are not available, however, other techniques are required.

Equation (2) implies that flows parallel to the magnetic field cannot affect its time derivative. To the extent that this approximation is valid, flows parallel to the field are completely unconstrained by both LCT applied to magnetograms and equation (4). We therefore assume that

$$\boldsymbol{v} \cdot \boldsymbol{B} = 0. \tag{6}$$

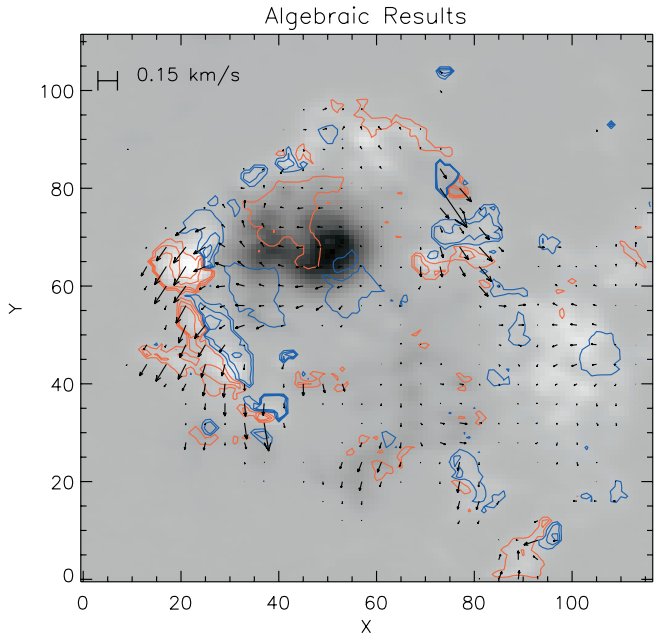

FIG. 5.—Results from the algebraic decomposition method applied to AR 8210. Vectors show horizontal velocities. (Vector density is reduced for visualization.) Blue (red) contours depict velocities toward (away from) the observer. Contour levels correspond to ±8, ±25, and ±41 m s^{-1}.

We recognize that, in general, $\boldsymbol{v}\cdot\boldsymbol{B}$ does not vanish; however, since the presence or magnitude of the flow along field lines has no bearing on the temporal evolution of the magnetic field (as described by the ideal MHD induction equation), we are free to adopt equation (6) to close the system.

This assumption, combined with equation (1), then yields simple algebraic relations that determine $\boldsymbol{v}$,

$$\boldsymbol{v}_t = \boldsymbol{u}^{(\mathrm{LCT})} - \frac{\left[\boldsymbol{u}^{(\mathrm{LCT})}\cdot\boldsymbol{B}_t\right]}{|\boldsymbol{B}|^2}\boldsymbol{B}_t \tag{7}$$

$$v_n = -\frac{B_n}{|\boldsymbol{B}|^2}\left[\boldsymbol{u}^{(\mathrm{LCT})}\cdot\boldsymbol{B}_t\right]. \tag{8}$$

We show results for this algebraic decomposition (ADC) method applied to AR 8210 in Figure 5, using $\boldsymbol{B}$ from 19:40 UT and $\boldsymbol{u}^{(\mathrm{LCT})}$ from correlating the B_z at 17:13 and at 21:29 UT.

Since the field evolution from ADC-derived velocities is exactly consistent with that from LCT, $-\nabla\cdot[\boldsymbol{u}^{(\mathrm{LCT})}\bar{B}_z]$, it is inconsistent with the actual normal field evolution, $\Delta B_z/\Delta t$. The differences between the ADC/LCT field evolution and actual field evolution can be seen by comparing the right panels of Figures 4 and 1, respectively.

3.4. *ILCT: Applying the Induction Equation*

To drive an MHD simulation with vector magnetograms, it is necessary to supply an electric field at the lower boundary [obtained from the velocity field via $\boldsymbol{E} = -(\boldsymbol{v}\times\boldsymbol{B})/c$] that is physically self-consistent with the evolution of the magnetic field observed at the photosphere. In practice, MHD codes often require the specification of certain components of the magnetic field and flow in a boundary *layer* to update the temporal evolution of all three components of the magnetic field consistently, while not overspecifying the hyperbolic system of equations. Since it is difficult to routinely obtain simultaneous vector magnetic field measurements at different heights in the atmosphere (e.g., at both the chromosphere and photosphere), we are unable to observationally obtain the vertical gradients necessary to "realistically" update the transverse components of the field.

We can, however, ensure that a flow field obtained from observations of the photosphere satisfies at least the vertical component of the ideal MHD induction equation—that it matches $\Delta B_z/\Delta t$. This observationally determined flow field can then be incorporated directly into an MHD boundary-updating scheme that will, no doubt, contain additional idealizations that allow for the self-consistent evolution of the photospheric boundary layer.

Kusano et al. (2002) developed a method for determining the photospheric flow field consistent with both LCT results and equation (4). Their technique expresses the electric field at the photosphere in terms of scalar and vector potentials, ϕ and $\boldsymbol{A}$, respectively, and uses an iterative approach to solve for ϕ. We have developed our own technique to derive flow fields consistent with both equation (4), the induction equation, and LCT results. Adding I (for the induction equation) to LCT, we have dubbed our method "ILCT." Unlike the approach of Kusano et al. (2002), ILCT uses only standard Fourier and algebraic methods in two dimensions, and is therefore fast and easily implemented.

Our solution method uses $\Delta B_n/\Delta t$ and $\boldsymbol{u}^{(\mathrm{LCT})}\bar{B}_n$ to separately constrain the recovered magnetic intensity flow pattern, $\boldsymbol{u}^{(\mathrm{REC})}$, where (REC) distinguishes the recovered field $\boldsymbol{u}^{(\mathrm{REC})}$ from the actual, unknown field $\boldsymbol{u}$. We begin by decomposing the vector field

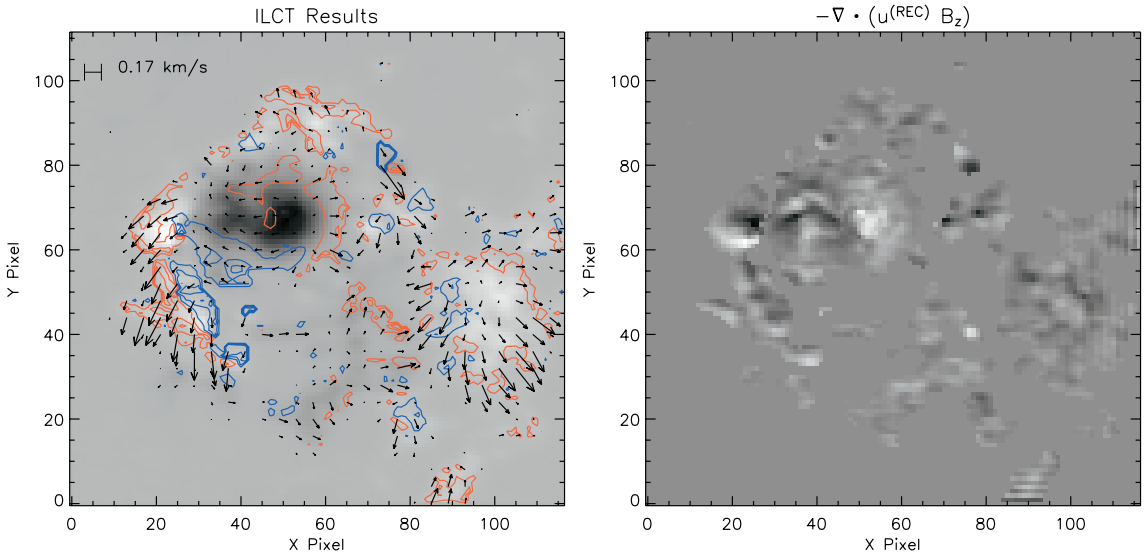

FIG. 6.—Results from the ILCT method applied to AR 8210. *Left*: Vectors show horizontal velocities (vector density is reduced for illustrative purposes). Blue (red) contours depict velocities toward (away from) the observer. Contour levels correspond to ±18, ±55, and ±92 m s^{-1}. *Right*: Gray scale of $-\nabla \cdot [\boldsymbol{u}^{(\mathrm{REC})} B_z]$, as defined by eq. (12) and computed from velocities at left. As expected, this matches the observed ΔB_z in the right panel of Fig. 1, apart from some Fourier ringing at the array's edges.

inside the divergence in the rightmost term of equation (5) into the sum of the curl of a stream function, ψ, and the gradient of a scalar function, ϕ,

$$\boldsymbol{u}^{(\mathrm{REC})}\bar{B}_n \equiv \nabla_t \times \psi\hat{\boldsymbol{n}} - \nabla_t\phi. \tag{9}$$

Plugging equation (9) into equation (4) results in a Poisson equation for ϕ,

$$\nabla_t^2\phi = \frac{\Delta B_n}{\Delta t}, \tag{10}$$

where $\Delta B_n/\Delta t$ acts as the source term. This equation is easily solved by standard Fourier techniques. Taking the curl of equation (9) and then dotting with the unit normal yields another Poisson equation, this one for ψ,

$$\nabla_t^2\psi = -\nabla_t \times \left[\boldsymbol{u}^{(\mathrm{REC})}\bar{B}_n\right] \cdot \hat{\boldsymbol{n}}. \tag{11}$$

We then use $\boldsymbol{u}^{(\mathrm{LCT})}$ as an estimate for $\boldsymbol{u}^{(\mathrm{REC})}$ in equation (11), which is also solved by standard Fourier techniques. Finally, we obtain our estimate of $\boldsymbol{u}^{(\mathrm{REC})}$ from equation (9). Because $\Delta B_n/\Delta t$ and $\boldsymbol{u}^{(\mathrm{LCT})}B_n$ are specified, equation (9) uniquely specifies $\boldsymbol{u}^{(\mathrm{REC})}\bar{B}_n$, if its values normal to the boundary are specified there. For strong fields lying entirely within the field of view, our reconstructed flows vanish on the boundary.

With these results, we verify that $-\nabla \cdot [\boldsymbol{u}^{(\mathrm{REC})}\bar{B}_n]$ accurately reconstructs $\Delta B_n/\Delta t$, as shown in the right panel of Figure 6. Comparison with the observed result, in the right panel of Figure 1, shows they only differ in some Fourier ringing at the array's edges in Figure 6. Note that, up to this point, no knowledge of the transverse field $\boldsymbol{B}_t$ is needed. Thus, the ILCT equations (9)–(11) can be used on line-of-sight magnetogram sequences, provided the surface normal and line-of-sight directions are not significantly inclined to the one another.

If vector magnetic fields are available, then we can make use of equations (1) and (6), which, combined with the definition

$$\boldsymbol{u}^{(\mathrm{REC})} = \boldsymbol{v}_t^{(\mathrm{REC})} - \left(\frac{v_n}{B_n}\right)^{(\mathrm{REC})}\bar{\boldsymbol{B}}_t, \tag{12}$$

allows us to solve the system for all three components of $\boldsymbol{v}^{(\mathrm{REC})}$. The flow field derived by this method is shown in the left panel of Figure 6. As in the algebraic decomposition method, we used $\boldsymbol{B}$ from 19:40 UT for $\bar{\boldsymbol{B}}$ and $\boldsymbol{u}^{(\mathrm{LCT})}$ from correlating B_z at 17:13 and at 21:29 UT. We remind the reader that only components of $\boldsymbol{v}$ normal to $\boldsymbol{B}$ can be recovered; no information on flows parallel to $\boldsymbol{B}$ can be determined from the induction equation.

4. DISCUSSION AND CONCLUSIONS

We have:

1. Presented our LCT technique, FLCT, and tested it by advecting a magnetogram with known velocity field and accurately recovering the imposed flow. We have also applied this method to a time series of vector magnetic field measurements of NOAA AR 8210, a CME-producing active region.

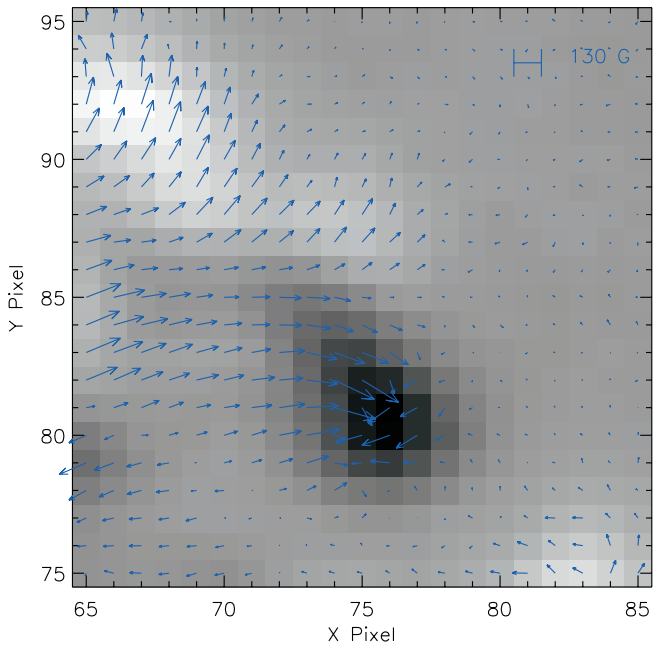

FIG. 7.—Magnetic field in a subregion of AR 8210 at 19:40 UT, near a fast-moving element of negative flux. The pixel labels demarcate the sub-region extracted from Fig. 1. Gray scale shows B_z; vectors show the tangential magnetic field. LCT shows the negative flux feature around {75, 81} headed down and right, while both algebraic decomposition and ILCT have an additional downflow on the feature's leading edge and an upflow on the feature's trailing edge, as can be seen in Figs. 5 and 6 (*left panel*).

2. Presented the algebraic decomposition method, ADC, which uses the relation derived by Démoulin & Berger (2003), to determine all three components of the photospheric velocity field after applying LCT to a time series of photospheric vector magnetograms.
3. Developed ILCT, a new method that determines a flow field consistent with both the vertical component of the ideal MHD induction equation and LCT applied to a time series of vector magnetograms.

We have applied each technique to AR 8210; however, ILCT is the only one of these three that provides a flow field suitable for incorporation into a data-driven MHD model of the solar corona.

We have compared our results with the evolution of features in the data movie of AR 8210 (available as an mpeg animation in the electronic version of this paper).[1] For instance, in the upper, central part of the field of view, an isolated, fast-moving negative flux concentration is seen to grow as it moves to the right and south, implying that flux is emerging there. Both the ADC and ILCT methods show an upflow in this region, consistent with our interpretation of the data. As the tangential field affects the derived up- and downflows in this region, we show the magnetic field there in more detail in Figure 7. In contrast, the LCT movie (available as an mpeg animation in the electronic version of this paper)[3] shows the same feature moving to the east at its emergence, then suddenly changing direction toward southwest. We believe the initial, eastward motion of the feature in the LCT movie is spurious, and results from newly emerged flux perturbing the cross-correlation.

As vector magnetogram coverage of eruptive events should improve in the near future, with NSF's SOLIS (Henney et al. 2002) and *Solar-B*'s Focal Plane Package (Tarbell 2002); these and other velocity-inversion methods will find wider use in studies of these events. Hence, improved understanding of flow-inversion techniques is essential. We are now testing the ILCT and algebraic decomposition techniques with three-dimensional MHD numerical simulations of photospheric and subphotospheric active region fields (Abbett et al. 2000, 2001; Bercik 2002), to characterize the strengths and weaknesses of these methods.

Our method of determining a velocity field says nothing about the forces (gas, magnetic, and radiative) that affect magnetic field evolution. Since enforcing consistency with only one component of the induction equation does not wholly constrain the photospheric velocity field, the most we can say is that our method generates a velocity field that is consistent with the evolution of the magnetic field's normal component.

As Démoulin & Berger (2003) implied, if chromospheric vector magnetograms could be coupled with photospheric vector magnetograms, then vertical derivatives of the field's components could be found, and the induction equation's other components could be used to further constrain the set of flows consistent with the observations. Such information would aid our effort to drive MHD simulations with data, since, in principle, we require boundary velocities consistent with the evolution of all three components of $\boldsymbol{B}$, not just B_n.

This work was supported by AFOSR, under a Department of Defense Multi-Universities Research Initiative (MURI) grant, "Understanding Solar Eruptions and Their Interplanetary Consequences," and by NSF, via the SHINE program, under ATM-0327712. Images used in the data and LCT movies were courtesy of the *SOHO* MDI research group at Stanford University. We have benefitted greatly from discussions with Dana Longcope on this topic at scientific meetings and at two MURI workshops. Some of the results presented here were inspired by Longcope's work on MEF, an alternative velocity-inversion technique. We are also grateful to Pascal Démoulin, whose helpful comments greatly improved the paper.

REFERENCES

Abbett, W., Fisher, G., & Fan, Y. 2000, ApJ, 540, 548
———. 2001, ApJ, 546, 1194
Auer, L. H., House, L. L., & Heasley, J. N. 1977, Sol. Phys., 55, 47
Bercik, D. J. 2002, Ph.D. thesis, Michigan State University
Berger, T. E., Loefdahl, M. G., Shine, R. S., & Title, A. M. 1998, ApJ, 495, 973
Canfield, R. C., de La Beaujardiere, J.-F., Fan, Y., Leka, K. D., McClymont, A. N., Metcalf, T. R., Mickey, D. L., Wuelser, J., & Lites, B. W. 1993, ApJ, 411, 362
Démoulin, P., & Berger, M. A. 2003, Sol. Phys., 215, 203
Démoulin, P., Hénoux, J. C., Mandrini, C. H., & Priest, E. R. 1997, Sol. Phys., 174, 73
Henney, C. J., et al. 2002, BAAS, 200, 55.14
Kupke, R., Labonte, B. J., & Mickey, D. L. 2000, Sol. Phys., 191, 97
Kusano, K., Maeshiro, T., Yokoyama, T., & Sakurai, T. 2002, ApJ, 577, 501
Landolfi, M., & Degl'Innocenti, E. L. 1982, Sol. Phys., 78, 355
Li, Y., Luhmann, J. G., Mulligan, T., Hoeksema, J. T., Arge, C. N., Plunkett, S. P., & St. Cyr, O. C. 2001, J. Geophys. Res., 106, 25103
Luhmann, J. G., Gosling, J. T., Hoeksema, J. T., & Zhao, X. 1998, J. Geophys. Res., 103, 6585
Mickey, D. L., Canfield, R. C., LaBonte, B. J., Leka, K. D., Waterson, M. F., & Weber, H. M. 1996, Sol. Phys., 168, 229
November, L., & Simon, G. 1988, ApJ, 333, 427
Pohjolainen, S., et al. 2001, ApJ, 556, 421
Régnier, S., Amari, T., & Canfield, R. C. 2002, in SOLMAG 2002, Proc. Magnetic Coupling of the Solar Atmosphere Euroconference (ESA SP-505; Garching: EAS), 65
Riley, P., Linker, J. A., & Mikic, Z. 2001, J. Geophys. Res., 106, 15889
Roussev, I. I., Gombosi, T. I., Sokolov, I. V., Velli, M., Manchester, W., DeZeeuw, D. L., Liewer, P., Tóth, G., & Luhmann, J. 2003, ApJ, 595, L57
Scherrer, P., et al. 1995, Sol. Phys., 162, 129
Simon, G. W., Brandt, P., November, L., Shine, R., & Strous, L. H. 1995, in Proc. 4th *SOHO* Workshop (Paris: ESA), 223
Sterling, A. C., & Moore, R. L. 2001, ApJ, 560, 1045
Sterling, A. C., Moore, R. L., Qiu, J., & Wang, H. 2001, ApJ, 561, 1116
Strous, L. H. 1995, in Proc. 4th *SOHO* Workshop (Paris: ESA), 219
Tarbell, T. 2002, EOS Trans. AGU, 83(19), SH31D–01
Unno, W. 1956, PASJ, 8, 108
Wang, T., Yan, Y., Wang, J., Kurokawa, H., & Shibata, K. 2002, ApJ, 572, 580
Warmuth, A., Hanslmeier, A., Messerotti, M., Cacciani, A., Moretti, P. F., & Otruba, W. 2000, Sol. Phys., 194, 103
Xia, Z., Wang, M., Zhang, B., & Yang, Y. 2002, Chinese Astron. Astrophys., 26, 164